Research Article

Banggui Guan*, Yanfu Qin, and Minglei Guo

Angle error control model of laser profilometer contact measurement

https://doi.org/10.1515/phys-2022-0062
received December 03, 2021; accepted June 20, 2022

Abstract: In controlling the angle error of laser profilometer contact measurement, the control model used in the past is subject to more external interference, which affects the measurement of other parameters, resulting in poor error control effect. Therefore, the angle error control model of laser profilometer contact measurement is designed by determining the initial zero position of the profilometer measuring sensor, compensating the nonlinear error, designing the interference signal processing circuit, and avoiding the error measurement influenced by external factors. From the main error sources such as the perpendicularity, standard error, sensor error and other errors of the coordinate axis of the profilometer, the accuracy is distributed. According to the equal action principle, the measurement uncertainty of the profilometer is calculated, and the measurement is obtained. According to the interference signal processing circuit and measurement index, the serial communication control circuit is designed, and the angle error control model of laser profilometer contact measurement is constructed. The experimental results show that the designed laser profilometer contact measurement angle error control model has high precision and does not affect other parameters in the control process, which shows that the control model has good effect in practical application.

Keywords: laser profilometer, contact measurement, angle error, control model

*** Corresponding author: Banggui Guan,** Department of Optoelectronic Engineering, School of Electrical and Electronic Engineering, Anhui Science and Technology University, Bengbu 233000, China, e-mail: gbg7712@163.com
Yanfu Qin, Minglei Guo: Department of Optoelectronic Engineering, School of Electrical and Electronic Engineering, Anhui Science and Technology University, Bengbu 233000, China

1 Introduction

With the continuous development of modern industrial technology, especially the continuous improvement of surface processing technology, and the continuous emergence of various types of complex parts, the demand for high-precision, large-scale measurement of part surface profile is more and more urgent. Especially in engineering applications, precision parts are generally contour surfaces with large curvature [1]. For example, in the optical application engineering, the surface profile of aspheric optical elements; in the aerospace industry, the complex surface of parts, in the mechanical engineering, the surface of rolling elements in the precision guide rail, *etc*. Different from the general smooth surface, the measurement of surface profile with large range and high precision not only requires that the surface roughness of the part should be measured accurately but also the waviness and shape error of the part surface should be measured. Because the traditional surface roughness profilometer only has a few millimeters of measuring range in the vertical direction, it is obviously difficult to meet the measurement requirements when measuring such a large curvature part. And when the measuring range of the measuring system is larger in the vertical direction, because this kind of measuring system adopts the measuring structure of lever contact pin type, with the increase in the lever angle, the angle of the lever around the fulcrum will be increased, which will lead to greater non-linear error, resulting in inaccurate measurement results. Because the material of the tip of the stylus is usually diamond, with the increase in the angle of the lever, the corresponding measuring force will increase, which will bring scratches to the surface of parts, especially the contour surface of parts with small rigidity. So, in the development of contour measurement, there must be a compromise between measurement accuracy, measurement range, and measurement force. For the contact measurement method, because of its principal error, it limits the development in the field of high-precision, large profile surface measurement. However, if the error model is

analyzed mathematically and the error curve is obtained, certain means and methods can be used to compensate the error, so as to meet the needs of large range and high precision measurement [2].

Profilometers can be classified into contact profilometer and non-contact profilometer according to the measurement methods. In the contact profilometer, the Zeiss F25 developed by Veghel M belongs to the contact linear measurement. Veghel not only defined the point-to-point calibration error of the three-dimensional space measuring machine but also evaluated the traceability of the measuring data points in the actual measurement of the measuring machine. The ultra-precision CMM developed by Ruijl has become the prototype of ISARA400, a high-precision contour measuring machine developed by IBS company. This measuring machine strictly follows the Abbe principle in the structural design, so there is no Abbe error. The stroke of ISARA400 is 400 mm × 400 mm × 100 mm, and the measurement uncertainty of perpendicularity is 0.025″. IBS has developed similar products with larger strokes. Because of its good repeatability, large measurement range, stable and reliable measurement results, low requirements on the surface of the workpiece to be measured, and high measurement accuracy, contact measurement method has been the most basic and widely used surface profile measurement method. Generally speaking, the principle of inductance, laser interference, and grating interference is used to detect the displacement of the contact profile measurement sensor. Due to the influence of nonlinear error, the measurement range of inductive sensor is limited, generally less than ±300 mm. Laser interference and grating interference sensors are based on the principle of laser interference length measurement, with high measurement accuracy and large measurement range, especially the micro displacement sensor based on cylinder grating interference, with the measurement range up to tens of millimeters, which can fully meet the requirements of surface profile measurement. However, when the laser profilometer is used to measure the angle, the control of angle error needs to be realized by the control model of measuring angle error. In ref. [3], a small angle measurement model of laser auto-collimation based on the common path compensation method is proposed. The measurement beam and the reference beam generated by this method can travel along approximately the same path, making the drift in the two beams almost equal. Therefore, the angle drift of the measurement beam can be fully compensated by the angle drift of the reference beam. The principle of compensation is analyzed. The experimental results show that the static measurement stability is better than 0.193 arc seconds and the compensation rate is greater than 86.6% in 100 min after compensation under 3 kinds of air parameter interference. In addition, 50 s after compensation, the dynamic measurement stability is 0.227 arc seconds, and the compensation rate is 53.6%. It is proved that the method is effective for laser autocollimation. In ref. [4], a calibration model for angle measurement accuracy of flexible support scanning device of space remote sensing camera is proposed. The zero position of scanning mirror is monitored by photoelectric autocollimator to solve the zero-position drift caused by theodolite over time and environment. According to the application requirements of high-speed rail, the necessity of subsection error compensation method is analyzed. The obtained angle error is introduced into the compensation system, and the angle measuring circuit is calibrated by the subsection error compensation method. By comparing the test results with the calibration results of harmonic error compensation method, it is verified that the angle measurement accuracy of the system can meet the requirements of the system performance index after segmented error compensation. Finally, the validity of the segmented error compensation method in the realization of high angle accuracy of limited angle scanning system of space remote sensing camera is determined. Ref. [5] studies the measurement error of laser instrument. In view of the fact that the laser instrument can carry out three-dimensional coordinate measurement in any position, this study first analyzes the basic meaning of the two terms “instrument angle” and “instrument apex angle,” and distinguishes the traditional “horizontal angle” and “vertical angle.” Based on the law of error propagation and the nominal accuracy of measuring angle and ranging, the point measuring error of laser instrument is analyzed. Taking the laser instrument Leica AT930 as an example, the disparity between “linear error of measuring angle” and “ranging error” is analyzed, and the measurement error control of laser instrument is realized. However, this method has poor ability to resist external interference, which leads to poor error control effect. Ref. [6] studies the high precision laser instrument error compensation technology. This error control method studies the calibration based on the turntable. By using the system-level calibration method, the calibration parameter error compensation model is established and the convergence parameter of Kalman filter is used to get more accurate calibration parameters. Finally, the system calibration of the laser instrument is carried out, but the error control method has the problem of large measurement error and poor compensation effect.

The above two models have obvious control effect on the measurement angle error, but they are easy to be

interfered with other parameters, resulting in large measurement and positioning error, and the model accuracy is difficult to be maintained at high level continuously, at the same time, it also affects the angle accuracy before and after the standard parts are reshaped [7–10]. In view of this situation, this work studies the angle error control model of laser profilometer contact measurement, and uses a higher level control model to solve the above problems.

2 Design of angle error control model for contact measurement of laser profilometer

2.1 Determining the initial zero position of the measuring sensor

The initial zero position of contact profilometry sensor affects the measurement accuracy and sensitivity of laser profilometer to a great extent, and the analysis of nonlinear error of measurement sensor is based on the premise that the sensor is in the initial zero position. If the initial zero position cannot be determined, then it will seriously affect the effect of non-linear error compensation. It directly affects the accuracy of measurement results. So how to find the zero position of the sensor quickly and effectively is very important. For this reason, a two quadrant photocell is proposed to detect the zero position of lever, and the method is shown in Figure 1.

According to the schematic diagram of detecting the zero position of the two-quadrant photoelectric tube, a two-quadrant photo electric detector is installed at the end of the lever. When the emitted laser is incident on the spectroscope 2, the reflected light will be incident on the two-quadrant photoelectric detector through the mirror 2. When the light intensity on the two quadrants is detected to be the same, that is to say, the output electric signal will be zero after the difference, this position will be marked as zero. However, due to the influence of the surrounding environment, the laser spot will drift irregularly, this is because the lase irradiation is not flat due to the laser speckle imaging, indicating that there will be no full reflection. Light from different directions corresponding to different representations will interfere when they meet in space. Because of the uneven representation, there will be a phase difference of light everywhere and thus interference, the light phase difference of different interferences may change, which will lead to a certain deviation of the zero position of the lever, so that the measurement results are not accurate. Since the sensor needs to be adjusted to the initial zero before each measurement, the zero detection must be simple, efficient, and easy to operate. Considering comprehensively, photoelectric switch is selected for zero position detection. The photoelectric switch transforms the change in light intensity between the transmitter and the receiver into current to achieve the purpose of object detection. Because the output circuit and the input circuit of the photoelectric switch are electrically isolated, they can be used in many applications. Moreover, the new generation of photoelectric switch has a series of advantages, such as delay, broadening, external synchronization, anti-interference, high reliability, and so on. Considering the structure of the sensor, the Omron counter proximity switch EE-SX670 is selected in the model design. The opposite type proximity

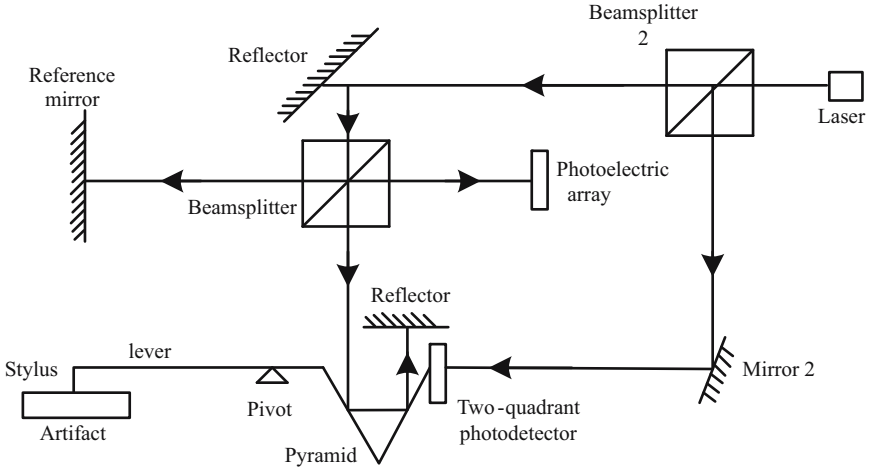

Figure 1: Schematic diagram of zero position detection structure of two-quadrant photoelectric cell.

switch is composed of two parts: emitter and receiver. When the beam is blocked by an object and interrupted, a change in the switch signal will be generated. By detecting the change in the switch signal, we can determine whether the sensor reaches the initial zero position [11–13]. The response frequency of OMRON EE-SX670 proximity switch is 1 kHz. Its characteristic curve is shown in the Figure 2.

It can be seen from the figure that when the photoelectric switch is in the on state, the output signal of the photoelectric switch is of low level; when the light beam is blocked by an object, the photoelectric switch will send out a high-level signal. By detecting the change in the high- and low- level signals, we can detect whether the sensor is at the initial zero position. Under the working environment of 25°C, the repeated response error of EE-SX670 is 2 mm, which can fully meet the accuracy requirements. Install the light baffle at the back end of the lever. When the lever rotates around the center support, the baffle will move with it. When the baffle rises or falls to a certain position, the photoelectric proximity switch will be triggered to determine the initial zero position of the profilometer measuring sensor.

2.2 Design of interference signal processing circuit

The interference signal processing circuit mainly includes direction identification, subdivision, and counting of the interference signal. The interference signal is received by four-quadrant photodiode, which is photoelectrically converted, and then after signal amplification, DC signal isolation, and zero crossing comparison processing, two orthogonal electrical signals are generated [14–17]. On the one hand, the signal enters the programmable logic controller (PLC) to subdivide the fringe signal and judge the moving direction; on the other hand, the signal passes through the A/D converter and gets the phase information through sampling. Finally, the signal is processed by computer to get the surface information of the measured work piece (Figure 3).

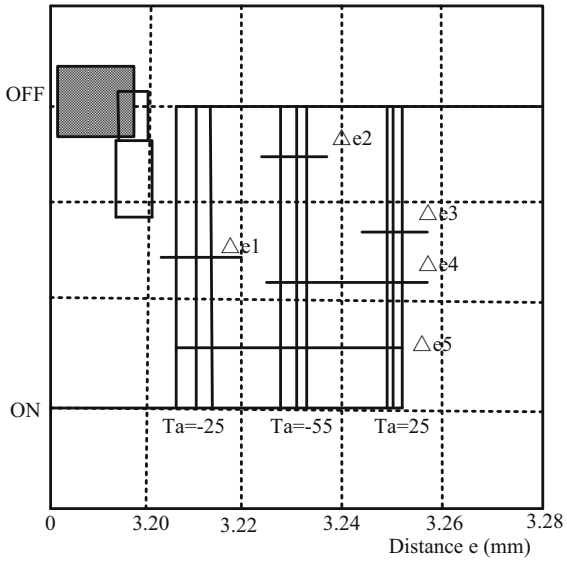

Figure 2: Omron repeatability curve.

In the laser profilometer, He–Ne laser is used as the laser power, and its wavelength is $\gamma = 632.8$ nm. According to the Michelson interference principle, the measurement distance is related to the half wavelength of the light source. Since the measurement beam needs to pass through the corner prism twice, the measurement resolution is 632.8/4 = 158.2 nm. However, the current output from the four-quadrant photodetector, after the first stage operational amplifier, will pass through the subsequent circuit. The reliability of the output signal in the first stage amplifier directly affects the stability of the final output signal of the laser profilometer, which leads to the decrease in the measurement accuracy. In order to avoid the influence of external factors on error measurement, it is necessary to adopt a method of combining circuit subdivision and computer subdivision, because circuit subdivision and computer subdivision can effectively reduce external interference according to the error source, so as to reduce the error, and can interpolate the periodic signal, so as to improve the resolution. The single chip microcomputer is used to count, identify direction, and subdivide the four subdivisions of interference signal, which is realized by the PLC GAL16V8 [18,19]. Then, the signal is converted by a 12 bit A/D conversion chip AD1674, and the sampling value is read by the computer. Since the A/D conversion chip AD1674 is 12 bits, the signals can be theoretically subdivided within 1/4 fringe period 212, and the theoretical resolution of the whole circuit is:

$$632.8 \times \frac{1}{4} \times \frac{1}{4} \times \frac{1}{2^{12}} \approx 0.01\,\text{nm}. \tag{1}$$

Considering the influence of asynchronous AD sampling and circuit interference, it is difficult to achieve theoretical resolution in practical measurement. However, in practical use, the resolution of the profilometer measurement system in the vertical direction is required to be 5 nm, so as long as 10 times subdivision is used, the accuracy requirements can be met, and the stability of the final output signal of the laser profilometer measurement sensor can be improved.

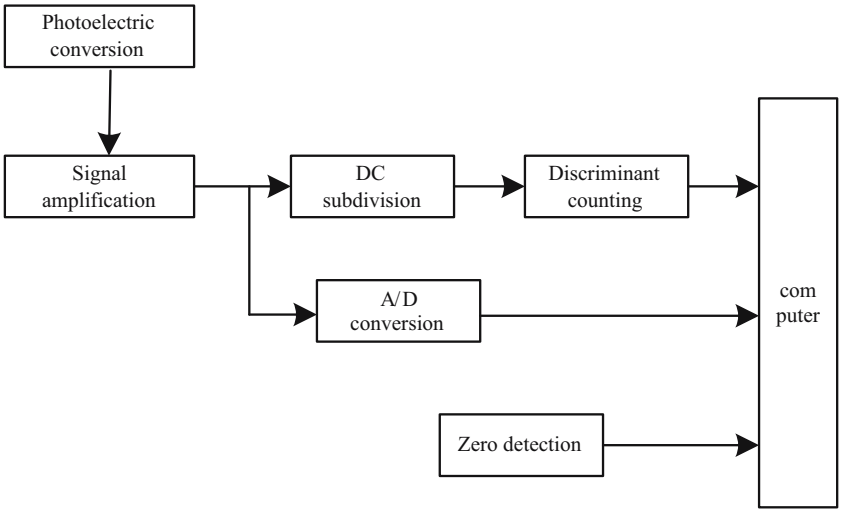

Figure 3: Schematic diagram of circuit structure.

2.3 Calculation of the measurement index of profilometer

In order to meet the actual measurement index of laser profilometer, the influence of other error factors on the surface error of profilometer shall be considered comprehensively in the actual error distribution and design. According to the principle of equal action, the design value of profilometer measurement accuracy is 0.5 mm. Assuming that the error distribution is in positive proportion to the travel axis, then the ratio of *X*:*Y*:*Z* is 8:8:1, and the calculation formula of error ξ_z obtained by *Z* axis distribution is:

$$\xi_z = \sqrt{\frac{\alpha^2}{0.5}}, \tag{2}$$

where α represents the measurement uncertainty of the profilometer, and 0.5 represents the design value of measuring precision of the profilometer. According to the proportion $\xi_x = \xi_y = 8\xi_z$, for *X*, starting from the main error sources such as perpendicularity, standard error, sensor error, and other errors of the coordinate axis of the profilometer, the accuracy distribution ξ_i is carried out according to the equal action principle, namely:

$$\xi_i = \sqrt{\frac{\xi_x^{\,2}}{6}}, \tag{3}$$

where *i* is the number of main error sources, and 6 indicates the upper limit of the number of major error sources. All errors are calculated by the above formula, and the variation range of errors is obtained. As the uncertainty assessment types are divided into class A and class B, when estimating each error component, it is necessary to select the appropriate assessment type to calculate the uncertainty in combination with the characteristics of the error itself [20–22]. So, the accuracy estimation process of *X* axis is as follows:

1) Verticality. If the final perpendicularity of the guide rail is controlled within 0.1″ after compensation, an uncertainty of about 0.19 mm will be generated within 400 mm stroke range.
2) Abbe error. Abbe error is caused by the non-collinearity of the probe axis and the grating reference line. The distance between the two and the pitch and angle errors of the *XY* axis determine the Abbe error. The pitch angle error of the guide rail is generally measured by laser interferometer or photoelectric autocollimator, and the corrected uncertainty depends on the measurement accuracy, repeatability error, and the distance from the measurement point to the grating. The measurement accuracy of laser interferometer in *X* direction is about 0.1″, the measurement accuracy of laser interferometer in *Y* direction is about 0.1″, and the distance between *X*-axis probe and grating is about 200 mm (the maximum distance between the probe and the other side of *X*-axis grating).
3) Straightness of guide rail. The uncertainty is determined by the straightness error and repeated measurement error. Because the straightness of the guide rail is about 0.1 M/250 mm and the repeated measurement error is about 0.03 mm, the combined straightness is about 0.1 M.
4) Standard error. This error is also composed of the indication error and repeatability error of grating, in which the indication error of grating is about 0.15 m and the repeatability error of grating is about 0.06 mm. So, the size is about 0.16 mm.

5) Sensor error. The sensor error depends on the accuracy index of the measurement sensor, and is also determined by the repeatability and stability of the measurement. Because the laser sensor is used in the measuring head of the laser profilometer, the measurement stability is 0.023 mm, and the measurement repeatability error is 0.017 mm, so the error is about 0.2 mm.
6) Other random errors. These errors include temperature errors caused by ambient temperature, electrical control errors, and some unknown errors. Because it is difficult to control these errors by external conditions, a large space can be reserved for this error distribution, and the error range is set to 0.2 m.

Based on the above, the precision design value of X axis is:

$$\xi_{\text{ep}} = \sqrt{\sum_{i=1}^{I} \xi_i^2}, \tag{4}$$

Bring the above specific values into the formula to get the precision design value of X-axis. When $\xi_{\text{ep}} \le \xi_i$, the distribution value of the above precision meets the requirements of measurement precision design index; when $\xi_{\text{ep}} = \xi_i$, and other distribution errors other than perpendicularity remain unchanged, the maximum allowable perpendicularity calculated is 0.1″. Therefore, when the verticality of laser profilometer is less than 0.1″, it can meet the accuracy index of profilometer measurement. According to the interference signal processing circuit and measurement index, the serial communication control circuit is designed, and the angle error control model of laser profilometer contact measurement is constructed to control the angle error of laser profilometer contact measurement.

2.4 Control circuit

The control circuit is mainly responsible for controlling AD converter and serial port, collecting data, and transmitting it to the upper computer, and the contact measurement controls the angular error. According to the requirements of various functions of the measurement system, adhering to the concept of making full use of resources and making smart use of resources, the main control unit selects the 8-bit, high-performance microprocessor ATmegal6 developed by ATMEL company. AVR kernel has rich instruction set and 32 general working registers. All registers are directly connected to the arithmetic-logic unit, so that one instruction can access two independent registers in one clock cycle. This architecture greatly improves the code efficiency and has a data throughput of up to ten times higher than that of the general CISC microcontroller. The overall architecture of the control module is shown in Figure 4.

The AD chip used in the control circuit is a 16 bit, four channel conversion Cs5523. Cs5523 is a high precision Δ – ΣA/D digital to analog converter with charge balance technology. Chopper stability measurement amplifier has

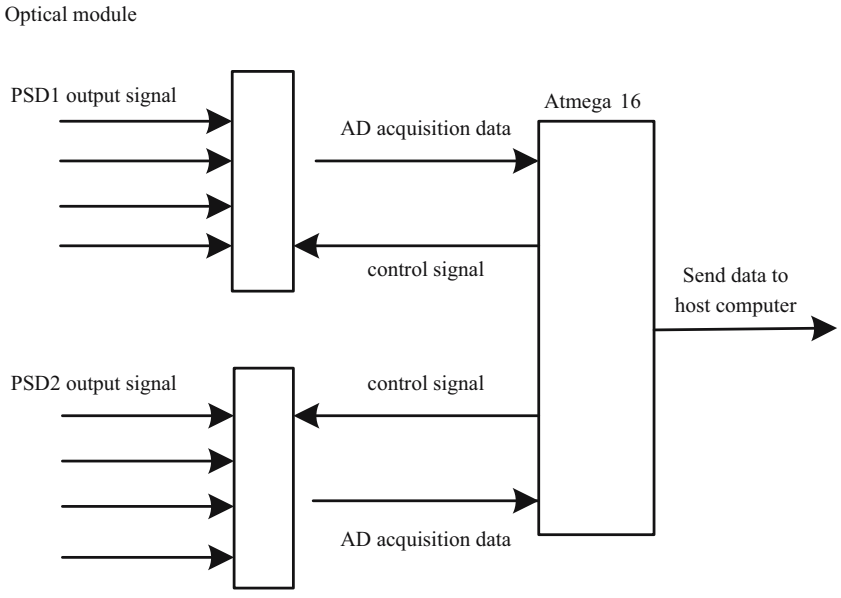

Figure 4: Overall structure of control module.

low input current with optional input range of 25, mV 55 mV, 100 mV, 1 V, 2.5 V, and 5 V. The amplifier has an AD converter has a programmable gain amplifier and a charge pump driving circuit which can provide negative power for its on-chip amplifier, so that the amplifier can measure the ground reference bipolar signal; at the same time, it also has a fourth-order $\Delta - \Sigma$-mode/modulator and a digital filter. Its digital filter provides eight programmable output update rates, and its filter can achieve complete accuracy for the selected output update rate in a conversion cycle. The filter can suppress both 50 and 60 Hz online interference when operating at 30 Hz or lower.

The connection between each unit in the control module is mainly realized through SPI interface. SPI is a synchronous serial communication mode introduced by Motorola Company and a three-wire synchronous bus. Because of its strong hardware function, the software related to SPI is quite simple, so that the CPU has more time to process other transactions.

The communication principle of SPI is very simple, and it works in the master-slave mode. This mode usually has one master device and one or more slave devices, which requires at least four lines. In fact, three lines can also be used (one-way transmission). It is also common to all SPI based devices. They are SDI (data input), SDO (data output), SCK (clock), and CS (chip selection). SDO and SDI are the data output and input of the main equipment, respectively, SCLK is the clock signal, which is generated by the main equipment, CS is the enabling signal of the slave equipment, which is controlled by the main equipment. CS is to control whether the chip is selected, that is to say, only when the chip selection signal is a predetermined enable signal (high potential or low potential), the operation of the chip is effective. This allows multiple SPI devices to be connected on the same bus. The serial communication control circuit is shown in Figure 5.

SPI communication is completed through data exchange. Here we need to know that SPI is a serial communication protocol, that is to say, data is transmitted one by one. This is the reason why SCK clock line exists. SCK provides clock pulse, and SDI and SDO complete data transmission based on this pulse. The data output is through the SDO line. The data change when the clock rises or falls, and is read at the next falling or rising edge. To complete one bit data transmission, input uses the same principle. In this way, the transmission of 8-bit data can be completed after at least 8 times of clock signal changes (the upper edge and the lower edge are once). It should be noted that the SCK signal line is only controlled by the master device, and the slave device cannot control the signal line. Similarly, in an SPI-based device, there is at least one master device. This kind of transmission mode is different from ordinary serial communication. Ordinary serial communication continuously transmits at least 8 bits of data at a time, while SPI allows data transmission of 1 bit at a time, or even allows pause. Because the SCK clock line is controlled by the master control device, when there is no clock jump, the slave device does not collect or transmit data. That is to say, the main equipment can control the communication by controlling the SCK clock line. SPI is also a data exchange protocol; because the data input and output lines of SPI are independent, it is allowed to complete the data input and output at the same time.

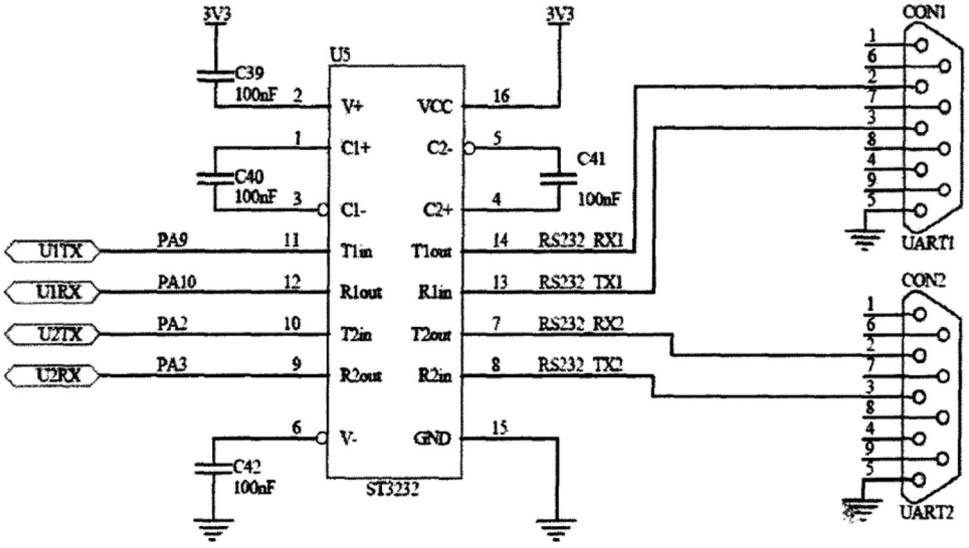

Figure 5: Serial communication control circuit.

Different SPI devices have different implementation methods, mainly due to different data change and acquisition times. There are different definitions for upper or lower edge acquisition of clock signal. Therefore, in practical application, appropriate SPI devices are selected according to actual needs.

The serial communication module configures the SPI communication mode by configuring the SSM bit of the SPI-CR1 register, and sets the DFF bit to define the data frame format as 8 or 16 bits. In addition, it also uses the 16 baud rate register and the highest baud rate selection. The data serial communication module consists of a start bit, a parity bit, a stop bit, and eight data bits. The baud rate used for communication is calculated as follows:

$$\mathrm{SPI} = \frac{\mathrm{SCK}}{(\mathrm{BRR} + 1) \times 8}, \tag{5}$$

According to formula (5), we can get:

$$\mathrm{BRR} = \frac{\mathrm{SCK}}{\mathrm{SPI} \times 8} - 1, \tag{6}$$

where SCK represents the frequency of peripheral communication clock, and the value of BRR register determines the baud rate. In this design, the BRR value is set to 243 to realize communication at 19,200 baud rate.

Through the design of the serial communication control circuit, the control model of the angle error of the laser profilometer contact measurement is constructed. The expression is as follows:

$$F_{\mathrm{SPI}} = \frac{\xi_{\mathrm{ep}}}{\mathrm{BRR} \times 8}, \tag{7}$$

In point-to-point communication, SPI interface does not need addressing operation, and it is full duplex communication. In the process of laser profilometer contact measurement angle error control, it can better ensure the real-time communication of each module, and control the laser profilometer contact measurement angle error.

3 Experimental results and analysis

3.1 Experimental platform and parameter setting

In order to verify the performance of the angle error control model of laser profilometer contact measurement in practical application, this work mainly studies the accuracy of the model, positioning error, and the angle accuracy of standard parts. In the study, the designed angle error control model of laser profilometer contact measurement is compared with the traditional small angle measurement model of laser auto-collimation based on common path compensation method and space remote sensing camera deflection. In the experiment, the laser profilometer is connected with the local computer interface, and the network browser is used in the remote man–machine interface, as shown in Figure 6.

The laser profilometer used in the experimental study includes vision controller and displacement sensor heads

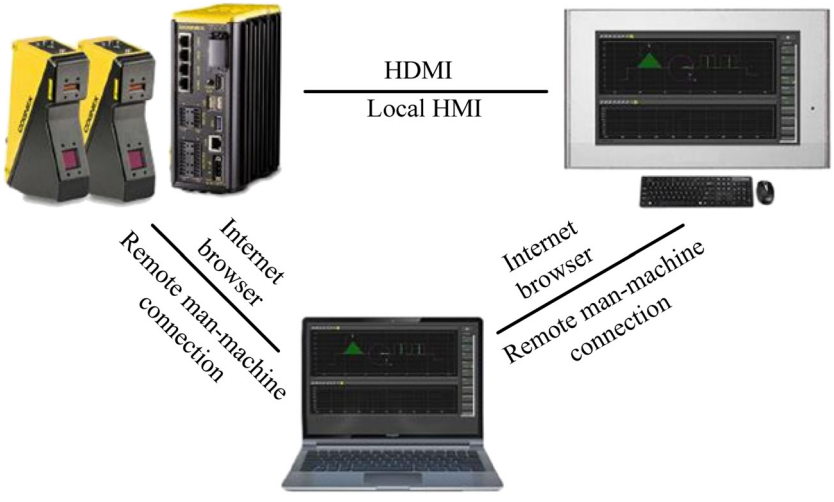

Figure 6: Connection diagram of laser profilometer.

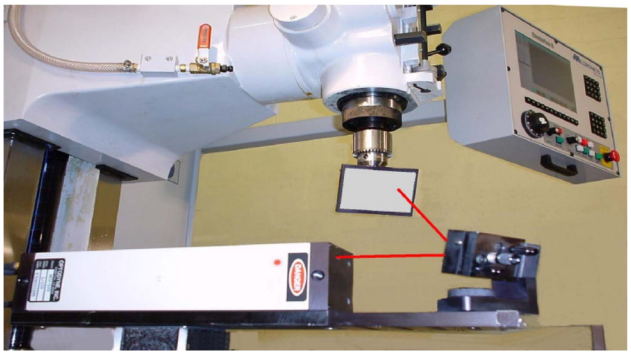

Figure 7: Experimental platform.

Table 1: Experimental parameter settings

Physical focal length	300 mm
Physical caliber	500 mm
Measuring distance	Maximum 25 mm
Maximum reading field	3,000″
Maximum measurement range	±1,000″
Resolving power	0.1″
Measurement accuracy	±0.3″
Communication interface	USB2.0

of different specifications. The vision controller has 8 optical isolated discrete inputs and 16 optical isolated discrete outputs, which are directly connected with the laser displacement sensor head. Additionally, Ethernet power supply is provided, and wireless storage can be realized through remote network equipment. The laser profilometer provides a movable and platform independent vision for the experiment, and can access the HMI from any position of the network. The HTML user interface enables the user to monitor the use of the instrument from any computer, tablet, smart phone, or other mobile devices. The error measurement and compensation experiments are carried out on a X_yF_z three-axis vertical machining center with a space position error compensation function controller Siemens 840D. The experimental platform is shown in Figure 7.

Through the experimental platform, the experimental parameters are set as shown in Table 1.

3.2 Model accuracy

Accuracy refers to the degree of proximity between the measurement result, calculation value or estimated value, and the true value. Error refers to the difference between

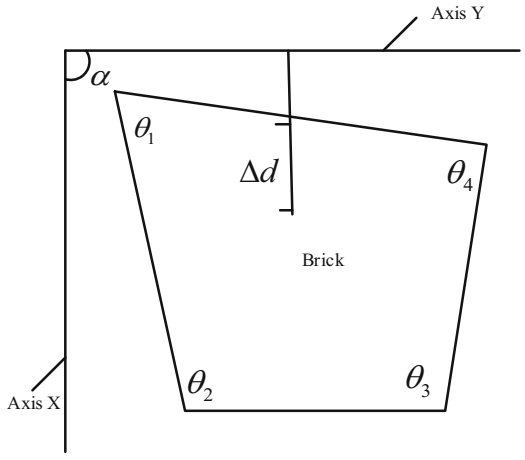

Figure 8: Verticality measurement error.

Table 2: Experimental results of model accuracy

Measuring position	Actual value (μm)	Measurement value of small angle measurement model of laser auto-collimation based on common path compensation (μm)	Measurement value of calibration model of angle measurement accuracy of flexible support scanning device of space remote sensing camera (μm)	The measurement value of angle error control model of laser profilometer contact measurement (μm)
1	1,000	997.643	999.105	999.998
2	2,000	1995.642	1998.254	1999.987
3	3,000	3002.647	3000.786	3000.012
4	4,000	4001.329	4001.678	4000.006
5	5,000	5003.231	5002.364	4999.976
6	6,000	5998.012	5997.071	6000.068
7	7,000	6995.214	6995.542	6999.924
8	8,000	8001.536	8002.247	8000.041
9	9,000	9002.347	9000.154	8999.992
10	10,000	9997.124	10000.789	9999.997

the measurement result or calculation value and the theoretical true value. Generally, the accuracy of the instrument can be expressed by the size of the error. In order to test the accuracy of the angle error control model of laser profilometer contact measurement designed in this work, it is necessary to calibrate the model with a higher accuracy measuring instrument. At the same time, the laser auto-collimation small angle measurement model based on the common path compensation method and the angle measurement accuracy calibration model of the flexible support scanning device of the space remote sensing camera are used for the accuracy comparison experiment. The results are shown in Table 2.

Observe the data in the table and calculate the precision errors of different models in different measuring positions. The calculation results show that the precision error of the laser auto-collimation small angle measurement model based on the common path compensation method is 2.546, the precision error of the calibration model of the angle measurement precision of the flexible support scanning device of the space remote sensing camera is 1.591, and the angle error control model of the laser profilometer contact measurement is calculated. Accuracy error of the model is 0.048. It can be seen from the calculation results that only the accuracy error of the angle error control model of the laser profilometer contact measurement designed in this work increases or decreases in the μm range, which meets the actual application requirements of the model.

3.3 Positioning error

The most direct effect of the level of the error control model of the laser profilometer on the contact measurement is the effect on the step value Δd, as shown in Figure 8.

In order to verify the validity of this model, the laser profilometer contact measurement angle error control model, the laser auto-collimation small angle measurement model based on the common path compensation method, and the laser profilometer contact measurement angle calibration model of the flexible support scanning device of the space remote sensing camera are positioned, and the positioning results are combined with the actual laser profilometer contact measurement angle positioning The results of error comparison are shown in Figure 9.

It can be seen from the results in the figure that the angle positioning results of the laser profilometer contact measurement of the angle error control model of the laser profilometer contact measurement are basically the same

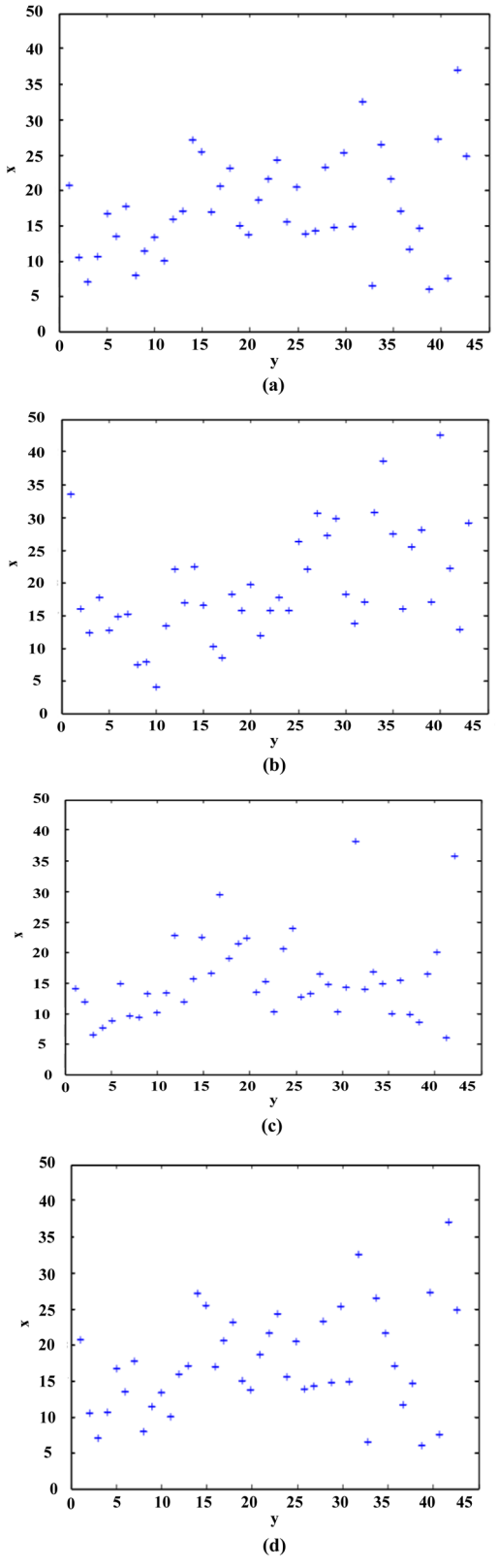

Figure 9: Positioning results of different models. (a) Actual positioning results. (b) Positioning results of small angle measurement model of laser auto-collimation based on common path compensation method. (c) Positioning results of calibration model of angle measurement accuracy for flexible support scanning device of space remote sensing camera. (d) The positioning results of the angle error control model for the contact measurement of the laser profilometer.

as the actual positioning results, while the contact measurement angle of the laser profilometer based on the small angle measurement model of the laser auto-collimation based on the common path compensation method and the angle accuracy calibration model of the flexible support scanning device of the space remote sensing camera is the same as the actual one The error of positioning results is large. To sum up, the designed control model has little influence on the positioning in the practical application process, and can control the angle error of the contact measurement of the laser profilometer within a reasonable range.

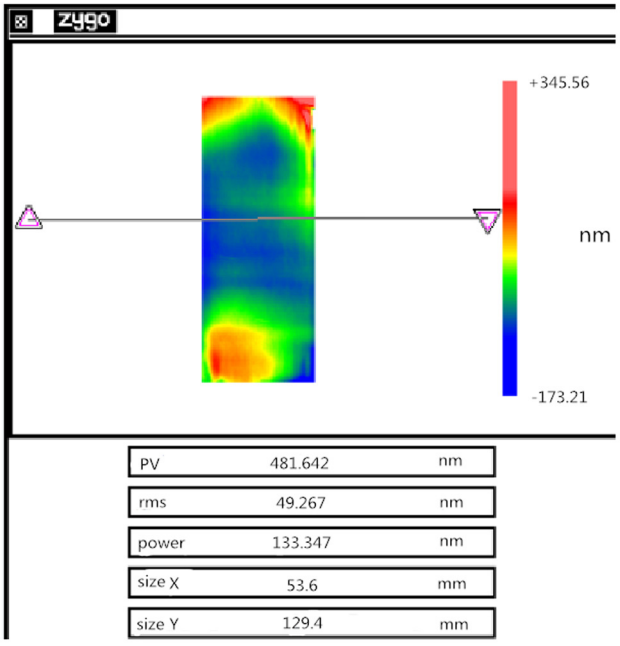

Figure 10: Shape data change state of square brick forming surface. (a) State of shape data changes during shape modification. (b) Modified surface shape data change state.

3.4 Angle accuracy of standard parts

In the angle accuracy experiment of standard parts, square bricks are selected as the object to be measured, and the theoretical accuracy of angle measurement can reach 0.5″. Using the existing processing and measuring equipment in the laboratory, the surface shape of square bricks and relevant angles are modified and improved until the actual accuracy reaches the accuracy required by the experiment. The initial shape accuracy of square brick is 125.69 nm for plane A, 854.23 nm for plane B, 712.36 pv for plane C and 147.71 pv for plane D. From the initial shape, the surface shape of the square brick is not ideal, and the flatness error is large, among which the flatness of B and C faces is the worst. Take the B-plane as the experimental object, and modify it first. The data of B-plane modification is as follows (Figure 10).

The change in peak value (PV) value during shaping is shown in the Figure 11.

After the modification, the four corners of the square brick before and after the modification are measured by using the laser profilometer contact measurement angle error control model, the laser auto-collimation small

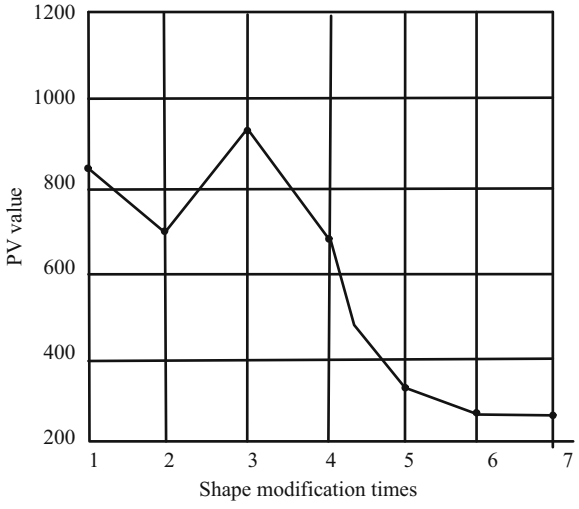

Figure 11: Analysis of the change in PV value.

Table 3: Size of peripheral angles of standard parts before and after reshaping

		θ_1	θ_2	θ_3	θ_4
Small angle measurement model of laser auto-collimation based on common path compensation	Before reshaping	89°45′15.61″	90°25′19.53″	89°51′23.65″	90°25′17.62″
	After reshaping	90°54′18.26″	89°06′16.45″	90°58′32.26″	89°01′22.34″
Calibration model of angle measurement accuracy for flexible support scanning device of space remote sensing camera	Before reshaping	89°15′36.47″	90°59′53.42″	89°2′14.63″	90°58′13.64″
	After reshaping	89°35′26.34″	90°23′11.24″	89°34′37.22″	90°16′41.25″
Angle error control model of laser profilometer contact measurement	Before reshaping	89°11′25.67″	89°13′28.57″	89°22′36.91″	89°16′19.26″
	After reshaping	90°09′07.63″	89°59′45.6″	90°03′32.24″	89°59′56.61″

angle measurement model based on the common path compensation method, and the angle measurement accuracy calibration model of the flexible support scanning device of the space remote sensing camera. The measurement results are as follows.

From the results in Table 3, it can be seen that there are differences in the angles before and after the modification of the square bricks measured by all models, which indicates that the surface shape of the square bricks has been effectively modified. Comparing and observing the measurement data of different models, there is a certain gap between the measurement results of the laser auto-collimation small angle measurement model based on the common path compensation method and the calibration model of the angle measurement accuracy of the flexible support scanning device of the space remote sensing camera and the results of the shape modification, especially the difference between the measured value after the shape modification and the actual right angle; compared with the difference, the contact measurement angle of the laser profiler is wrong. The measured value in the difference control model is closer to the actual data. Combined with the experimental results of model accuracy and positioning error results, it can be seen that the designed laser profilometer contact measurement angle error control model will not affect the change in other parameters in the actual work, and always maintain a high accuracy.

4 Conclusion

The measurement of contact angle of laser profilometer is a very important part in the field of laser detection. However, the traditional mechanical measurement method in optics cannot meet the requirements of measurement accuracy. With the development of electronic technology, optical sensors have been widely used to measure various physical quantities. In the process of laser profilometer contact angle measurement, the position and angle of beam incidence are very important physical quantities. Especially in the experiments that need precise alignment, the position and angle measurement of the incident beam need high precision. At the same time, in the experiment with high real-time requirements, the movement of the instrument and the time of replacing the instrument will have a serious impact on the experimental results, which requires that the instrument can measure the position and angle of the incident beam in real time. For this kind of situation, this work studies the laser profiler contact

measurement error control model, through the nonlinear error compensation, designed the interference signal processing circuit from the main error sources allocation according to the principle of precision, calculated the measurement uncertainty contour graph, and built the laser profiler contact angle measurement error control model. Through the experimental analysis, the accuracy error of the laser profiler contact Angle measurement error control model is only 0.048, and the orientation of contact angle measurement results and the actual results, at the same time in the practical work will not affect the change in other parameters, always maintain high precision, so the method to effectively control the laser profiler contact angle measurement error. It has good application effect and provides certain technical support for the research and development of laser profilometer in the future.

Funding information: The research was supported by: The Educational commission of Anhui province of China – Preparation and technology of super-resolution imaging microlens array films (No. KJ2020A0074).

Author contributions: All authors have accepted responsibility for the entire content of this manuscript and approved its submission.

Conflict of interest: The authors state no conflict of interest.

Data availability statement: The datasets generated during and/or analysed during the current study are available from the corresponding author on reasonable request.

References

[1] Tang K, Lv X, Wu S, Xuan S, Huang X, Bai C. Measurement for contact angle of iron ore particles and water. ISIJ Int. 2018;58(3):379–400.
[2] Prydatko AV, Belyaeva LA, Jiang L, Lima L, Schneider GF. Contact angle measurement of free-standing square-millimeter single-layer graphene. Nat Commun. 2018;9(18):3082–96.
[3] Guo Y, Cheng H, Wen Y, Wu H, Wu Y. Small-angle measurement in laser auto-collimation based on a common-path compensation method. J Mod Opt. 2019;66(18):1818–26.
[4] Chi DN, Xu LN, Zhao X, Zhang XQ, JIA HL. Calibration method for angle measurement accuracy of flexible support scanning device of space remote sensing camera. Space return Remote Sens. 2018;39(05):93–9.
[5] Liu D, Millimet DL. Measurement error analysis and accuracy simulation of laser tracker. Eng surveying Mapp. 2021;30(6):21–6.
[6] Luo T, Xie CC, Zhang J. Research on error compensation technology of high precision laser north finder. Piezoelectrics Acoustooptics. 2021;43(3):399–401, 405.
[7] Huang X, Cao M, Wang D, Li X, Fan J, Li X. Broadband polarization-insensitive and oblique-incidence terahertz metamaterial absorber with multi-layered graphene. Optical Mater express. 2022;12(2):811.
[8] Li H, Zhang Y, Tai Y, Zhu X, Qi X, Zhou L, et al. Flexible transparent electromagnetic interference shielding films with silver mesh fabricated using electric-field-driven microscale 3D printing. Opt laser Technol. 2022;148:107717.
[9] Li H, Li Z, Li N, Zhu X, Zhang Y, Sun L, et al. 3D printed high performance silver mesh for transparent glass heaters through liquid sacrificial substrate electric-field-driven Jet. Small (Weinh an der Bergstrasse, Ger). 2022;18:e2107811.
[10] Wang Q, Zhou G, Song R, Xie Y, Luo M, Yue T. Continuous space ant colony algorithm for automatic selection of orthophoto mosaic seamline network. ISPRS J photogrammetry Remote Sens. 2022;186:201–17.
[11] Moritz PKF, Michael R, Georg P. Global small-angle scattering data analysis of inverted hexagonal phases. J Appl Crystallography. 2019;52(2):403–14.
[12] Zhou G, Yang F, Xiao J. Study on pixel entanglement theory for imagery classification. IEEE Trans Geosci Remote Sens. 2022;60:1–18.
[13] Xiong Q, Chen Z, Huang J, Zhang M, Song H, Hou X, et al. Preparation, structure and mechanical properties of Sialon ceramics by transition metal-catalyzed nitriding reaction. Rare Met. 2020;39(5):589–96.
[14] Chen X, Wang Y, Zhu G, Zhang W, Zhou G, Fan Y. Influence of multi-angle input of intraoperative fluoroscopic images on the spatial positioning accuracy of the C-arm calibration-based algorithm of a CAOS system. Med Biol Eng Comput. 2020;58(7):559–72.
[15] Jens E, Rodolfo F. Weak mixing angle in the Thomson limit. J High Energy Phys. 2018;2018(3):1–23.
[16] Wu B, Xu Y, Yang FT, Qian CQ, Cai B. 3D coordinate measuring system based on laser tracking absolute length measurement multilateral method. Infrared Laser Eng. 2018;47(08):140–5.
[17] Yan Y, Feng L, Shi M, Cui C, Liu Y. Effect of plasma-activated water on the structure and *in vitro* digestibility of waxy and normal maize starches during heat-moisture treatment. Food Chem. 2020;306:125589.
[18] Li C, Zhou HB, Wang GL, Mu HZ, Li T. Research on fast recognition and location algorithm of photosensitive component in the laser rangefinder lens. Infrared Technol. 2019;41(01):35–43.
[19] Rueangsirarak W, Zhang J, Aslam N, Ho E, Shum H. Automatic comprehensive noncontact measurement and solution method for cylindrical workpieces without targets. Opt Precis Eng. 2018;26(12):2963–70.
[20] An R, Li ZR, Yang QG, Ye Y. Design principle and performance of RIXS spectrometer. High Power Laser Part Beams. 2018;30(07):7–14.
[21] Yang F, Fang AP, Xu SZ, Li Y. Accuracy evaluation of airborne LiDAR using the test field. Sci Surveying Mapp. 2019;44(06):193–7 + 241.
[22] Xie FP, Jiang WG. Simulation of single axis variable frequency tracking control for photovoltaic power generation system. Computer Simul. 2018;35(06):116–21 + 151.